Research Paper
J. Astron. Space Sci. 39(2), 35-42 (2022)
https://doi.org/10.5140/JASS.2022.39.2.35

JASS Journal of Astronomy and Space Sciences

Electromagnetic Electron-Cyclotron Wave for Ring Distribution with Alternating Current (AC) Electric Field in Saturn Magnetosphere

Annex Edappattu Haridas, Shefali Kanwar, Rama Shankar Pandey†
Department of Physics, Amity Institute of Applied Sciences, Amity University, Noida, Uttar Pradesh 201303, India

During their respective missions, the spacecraft Voyager and Cassini measured several Saturn magnetosphere parameters at different radial distances. As a result of information gathered throughout the journey, Voyager 1 discovered hot and cold electron distribution components, number density, and energy in the 6–18 Rs range. Observations made by Voyager of intensity fluctuations in the 20–30 keV range show electrons are situated in the resonance spectrum's high energy tail. Plasma waves in the magnetosphere can be used to locate Saturn's inner magnetosphere's plasma clusters, which are controlled by Saturn's spin. Electromagnetic electron cyclotron (EMEC) wave ring distribution function has been investigated. Kinetic and linear approaches have been used to study electromagnetic cyclotron (EMEC) wave propagation. EMEC waves' stability can be assessed by analyzing the dispersion relation's effect on the ring distribution function. The primary goal of this study is to determine the impact of the magnetosphere parameters which is observed by Cassini. The magnetosphere of Saturn has also been observed. When the plasma parameters are increased as the distribution index, the growth/damping rate increases until the magnetic field model affects the magnetic field at equator, as can be seen in the graphs. We discuss the outputs of our model in the context of measurements made in situ by the Cassini spacecraft.

Keywords: Saturn's magnetosphere, solar plasma, electron-cyclotron waves, the ring-distribution function

1. INTRODUCTION

Saturn's orbit has a volume (8.2713×10^{14} km^3) comparable to a small planetary system. Its environment is well-known for its complexity (Horner et al. 2020). This vast magnetosphere is divided by several zones and boundaries. The magnetosphere is made up of the cold plasma torus, inner magnetosphere (which contains the dynamic plasma sheet), and high-latitude magnetosphere, which has a magnetic field of 12–15 R_S (André et al. 2005). Telescopic observations and *in situ* measurements of the plasma torus have revealed that the density, temperature, and composition of the plasma torus vary over time, sometimes by a factor of two. (Delamere & Bagenal 2003) There are two main features of the inner plasma ring: low temperature and high equatorial density at 8 Rs. In plasma, sputtered water group ions detach from ice satellite, ring, and proton surfaces, causing the area to couple with the ring system. Plasma is mostly generated by ice satellites. This area is lacking in high-energy electrons. The electrons, plasma waves, plasma ions, and neutral gases interact to cause this loss. An extensive plasma sheet can be found between 8 and 15 R_S. The magnetic field data from the Cassini satellite's magnetometer was used to study the water group ion cyclotron waves in Saturn's magnetosphere. (Chou & Cheng 2017). Since the cold plasma composition is uniform throughout the magnetic layer, it shows that a mechanism is in place to rebalance all of the plasma in this region (Goertz 1983).

At low latitudes, Voyager 1 discovered irregularities in the plasma structure. Solar wind strength and Saturn's biggest moon Titan influence this region's structure (Eviatar et al. 1982). As opposed to cold plasma, which is restricted to the equatorial plane, hot plasma predominates in this region.

Whistler mode waves in the Earth's ionosphere were

Received 11 FEB 2022 **Revised** 06 MAR 2022 **Accepted** 28 MAR 2022
†**Corresponding Author**
Tel: +91-986-863-9418, E-mail: rspandey@amity.edu
ORCID: https://orcid.org/0000-0003-4907-1080

http://janss.kr pISSN: 2093-5587 eISSN: 2093-1409

first identified in the literature more than a century ago as electron cyclotron waves. The magnetosphere and plasmasphere of Earth are where scientists have found whistlers. Recent satellite missions, like as Cluster, Freja, and Polar, have discovered modulated whistler mode wave patterns that are linked to changes in density. Observations of whistler mode waves in the ionospheric density have been made during both natural and laboratory events. Wave particle interactions in circumterrestrial plasma can excite these waves. Gurnett et al. (1981) were the first to report on studies of Saturn's plasma wave spectrum made by Voyager 1. Gurnett & Bhattacharjee (2005) presented data from Saturn's approach and initial orbit for the first time in 2005 for "Cassini Radio and Plasma Wave Science Investigation." Following its orbit entry in July 2004, Cassini saw Saturn's magnetosphere for the first time. Using plasma data from Voyager 1 and 2, Richardson & Sittler (1990) were the first to show the ion electron densities in Saturn's inner magnetosphere in two dimensions. Calculations have been done in Saturn's magnetosphere like the ion total flux tube content, with the magnetic field model, we hope to study how electromagnetic electron cyclotron (EMEC) waves evolve in Saturn's magnetosphere. Cassini's magnetosphere measurements were used to derive the plasma's characteristics.

Using the Cluster/STAFF instrument, Lacombe et al. (2014) have observed narrowband, right-handed, circularly polarized fluctuations, with wave vectors quasi-parallel to the mean magnetic field, superimposed on the spectrum of the permanent background turbulence. We interpret these coherent fluctuations as whistler mode waves.

Based on previous studies and efforts to done comprehend electron cyclotron waves in the magnetosphere, an attempt was made to analyze the influence of obliquely propagating EMEC oscillations in Saturn's enormous magnetosphere on the growth rate. The primary goal of the study is to look at how EMEC waves are generated and what their effects are when different parameters are changed. The dispersion relation is incorporated into the study, which is presented in depth in the next part using the thorough formulation and mathematics employed.

2. MATHEMATICAL FORMULATION

Magnetic and electric fields should have the same z-direction in an anisotropic, collisionless, homogenous plasma system and magnitude $\mathrm{B} = \mathrm{B}_0\hat{\mathrm{e}}_z$ and electric field $\mathrm{E} = E_0 \sin \nu t\hat{\mathrm{e}}_z$. In the current circumstance, inhomogeneity in the interaction zone is expected to be minimal. The altered distribution function and particle trajectories associated with the dispersion relation are obtained using the Vlasov-Maxwell equations. Once the equilibrium and non-equilibrium components have been separated, higher order terms are removed.

The particle trajectories we estimated and, distribution functions, conductivity tensors, and dispersion relations using data from Annex & Pandey (2019) changed along with (equation 9):

The dielectric tensor is denoted by :

$$\varepsilon_{\mathrm{ij}}(k,\omega) = 1 + \sum_{\mathrm{s}} \left\{ \frac{4e_s^2\pi}{\mathrm{m_s}\omega^2} \right\} \sum_{\mathrm{n}} \sum_{\mathrm{p}} \mathrm{J_p}(\lambda_2) \int \frac{\mathrm{d^3v} \,\|\, \mathrm{S_{ij}^*} \,\|}{\omega - \mathrm{k_{\|}} \mathrm{v_{\|}} - \dfrac{\mathrm{k_{\|}}\Gamma_z}{\mathrm{v}} + \mathrm{p}\nu - \mathrm{n}\omega_{\mathrm{c}}} \tag{1}$$

where

$$\left\| \mathrm{S_{ij}^*} \right\| = \begin{vmatrix} \mathrm{v_\perp U^*} \left(\dfrac{\mathrm{n}}{\lambda_1} \right)^2 \mathrm{J_n^2} & \mathrm{i v_\perp U^*} \left(\dfrac{\mathrm{n}}{\lambda_1} \right) \mathrm{J_n J_n'} & \mathrm{v_\perp W^*} \left(\dfrac{\mathrm{n}}{\lambda_1} \right) \mathrm{J_n^2} \\ \mathrm{i v_\perp U^*} \left(\dfrac{\mathrm{n}}{\lambda_1} \right) \mathrm{J_n J_n'} & -\mathrm{v_\perp U^*} \left(\mathrm{J_n'} \right)^2 & \mathrm{i v_\perp W^* J_n J_n'} \\ \mathrm{v_{\|} U^*} \left(\dfrac{\mathrm{n}}{\lambda_1} \right) \mathrm{J_n^2} & \mathrm{i v_{\|} U^* J_n J_n'} & \mathrm{v_{\|} W^* J_n^2} \end{vmatrix}$$

Terms notation of the above equation have been defined in Annex & Pandey (2019).

The general dispersion relation is used to describe the propagation of electromagnetic electron cyclotron waves, which reduces to $\varepsilon_{11} \pm i\varepsilon_{12} = N^2\cos^2\theta$, N^2 being the refractive index which defined as $\mathrm{N}^2 = \frac{\mathrm{k^2c^2}}{\omega^2}$.

For oblique propagation and order of Bessel function n = 1, the dispersion relation with parallel AC electric field is as follows:

$$\frac{k^2 cos^2\theta c^2}{\omega^2} = 1 + \sum_s \frac{4e_s^2\pi}{\omega^2} \sum_p J_p(\lambda_2) \int \frac{d^3v}{2} v_\perp \left[\left(\omega - k_{\|} v_{\|} \right) \frac{\partial f_o}{\partial v_\perp} - k_{\|} \frac{\partial f_o}{\partial v_\perp} \frac{\Gamma_{\|s}}{\nu} \left(\frac{p}{\lambda_2} - 1 \right) + k_{\|} v_\perp \frac{\partial f_o}{\partial v_{\|}} \right] \times \left(\frac{1}{\omega - k_{\|} v_{\|} - \dfrac{k_{\|}\Gamma_{\|s}}{\nu} + pv \pm \omega_c} \right) \tag{2}$$

The distribution function of trapped electrons can be described as Maxwellian ring, as Wu et al. (1989) and Kumar et al. (2007)

$$f\left(v_{\perp}, v_{\parallel}\right)=\frac{n_s / n}{\pi^{3/2}\alpha_{\parallel s}\alpha_{\perp s}^2 A}\exp\left[-\frac{\left(v_{\perp}-v_o\right)^2}{\alpha_{\perp s}^2}-\frac{\left(v_{\parallel}^2\right)}{\alpha_{\parallel s}^2}\right] \quad (3)$$

$$A=\exp\left(-\frac{v_o^2}{\alpha_{\perp s}^2}\right)+\sqrt{\pi}\left(\frac{v_o}{\alpha_{\perp s}}\right)\operatorname{erfc}\left(-\frac{v_o}{\alpha_{\parallel s}}\right) \quad (4)$$

where s stands for species, and electrons and ions are considered in this example,

$$\alpha_{\parallel e}=\left(2k_b T_{\parallel e}/m_e\right)^{1/2},\ \alpha_{\perp e}=\left(2k_b T_{\perp i}/m_e\right)^{1/2},$$

$$\alpha_{\parallel i}=\left(2k_b T_{\parallel i}/m_i\right)^{1/2} \text{ and } \alpha_{\perp i}=\left(2k_b T_{\perp i}/m_i\right)^{1/2}$$

are the ions' and electrons' related parallel and perpendicular thermal velocities.

n_s/n Equation (3) The electron-to-total density ratio, which is caught and defined by high energy, is depicted, whereas erfc(x) is the error function itself. Magnetic fields are used to describe $v_{\perp}$ and $v_{\parallel}$ the thermal velocities in perpendicular and parallel directions, respectively. The drift velocity is denoted by v_o in the mathematical expression.

Substituting $d^3v=2\pi\int_0^{\infty}v_{\perp}dv_{\perp}\int_{-\infty}^{\infty}dv_{\parallel}$ and using expression (4) in equation (3) and after solving the integrations, we get the dispersion relation as:

$$\frac{k^2\cos^2\theta c^2}{\omega^2}=1+\frac{4e_s^2\pi}{\omega^2}\sum_p J_p\left(\lambda_2\right)\frac{\left(n_s/n\right)}{A}\left[\begin{array}{l}\frac{1}{\alpha_{\parallel s}}\left(\frac{\omega}{k_{\parallel}}-\frac{\Gamma_{\parallel s}}{\nu}\left(\frac{p}{\lambda_2}-1\right)\right)X_{1s}Z\left(\xi\right)\\+X_{2s}\left(1+\xi Z\left(\xi\right)\right)\end{array}\right] \quad (5)$$

To reduce above expression for electron-cyclotron range of frequencies, ion temperatures are assumed to be $T_{\perp i}=T_{\parallel i}=T_i$ and $|\omega_r+i\gamma|\ll\omega_{ci}$ while the electrons are assumed to have $T_{\perp e}>T_{\parallel e}$ along with $|k_{\parallel}\alpha_{\parallel e}|\ll|\omega_r\pm\omega_{ce}+i\gamma|$.

So, following these approximations, equation (5) is reduced to:

$$D\left(k,\omega_r+i\gamma\right)=1-\frac{k^2\cos^2 c^2}{\left(\omega_r+i\gamma\right)^2}\left[\begin{array}{l}\left\{\frac{\omega_{pi}^2}{\omega_{ci}^2}-\frac{\omega_{pi}^2}{\left(\omega_r+i\gamma\right)\pm\omega_{ci}}\right\}X_{1i}\\+\sum_p Jp\left(\lambda_2\right)\left[\begin{array}{l}+\frac{\omega_{pe}^2}{\left(\omega_r+i\gamma\right)^2}\left[\begin{array}{l}X_{1e}\frac{1}{\alpha_{\parallel e}}\left(\begin{array}{l}\frac{\omega_r+i\gamma}{k_{\parallel}}\\-\frac{\Gamma_{\parallel e}}{\beta v}\left(\frac{p}{\lambda_2}-1\right)\end{array}\right)Z(\xi)\\+X_{2e}\left(1+\xi Z(\xi)\right)\end{array}\right]\end{array}\right]\end{array}\right] \quad (6)$$

where

$$X_{1i}=1+\frac{v_o^2}{\alpha_{\perp i}^2}-\sqrt{\pi}\frac{v_o}{\alpha_{\perp i}},\ X_{1e}=1+\frac{v_o^2}{\alpha_{\perp e}^2}-\sqrt{\pi}\frac{v_o}{\alpha_{\perp e}} \text{ and}$$

$$X_{2e}=X_{1e}+\frac{\alpha_{\perp e}^2}{\alpha_{\parallel e}^2}\left(\begin{array}{l}1-\sqrt{\pi}\frac{v_o^3}{\alpha_{\perp e}^3}erfc\left(\frac{v'_{\perp e}}{\alpha_{\perp e}}\right)\\+3\frac{v_o^2}{\alpha_{\perp e}^2}-\frac{3}{2}\sqrt{\pi}\frac{v_o}{\alpha_{\perp e}}\end{array}\right)$$

We apply the condition $\frac{k^2\cos^2 c^2}{\omega^2}\gg 1+\frac{\omega_{pi}^2}{\omega_{ci}^2}$ and satisfying charge neutrality $\frac{\omega_{pe}^2}{\pm\omega_{ce}}=\frac{\omega_{pi}^2}{\pm\omega_{ci}}$ by Pandey & Kaur (2015) The dispersion relation is rewritten as:

$$D\left(k,\omega_r+i\gamma\right)=-\frac{k_{\parallel}^2c^2}{\omega_{pe}^2}+\sum_p J_p\left(\lambda_2\right)\left[\begin{array}{l}\left\{\frac{\omega}{\pm\omega_{ci}}\right\}X_{1i}\\+\left[\begin{array}{l}X_{1e}\frac{1}{\alpha_{\parallel e}}\left(\frac{\omega_r}{k_{\parallel}}-\frac{\Gamma_{\parallel e}}{\nu}\left(\frac{p}{\lambda_2}-1\right)\right)Z(\xi)\\+\frac{X_{2e}}{X_{1e}}\left(1+\xi Z(\xi)\right)\end{array}\right]\end{array}\right] \quad (7)$$

The plasma dispersion function is defined as follows:

$$Z\left(\xi\right)=\frac{1}{\sqrt{\pi}}\int_{-\infty}^{\infty}\frac{e^{-t^2}}{t-\xi}dt,$$

$$\text{where } \xi=\frac{\omega-k_{\parallel}\Gamma_{\parallel s}/v+pv\pm\omega_c}{k_{\parallel}\alpha_{\parallel s}},\ \ \omega_{ps}^2=\frac{4\pi e_s^2 n_s/n}{B}$$

Now, the dimensionless parameter $\tilde{k}=\frac{k_{\parallel}\alpha_{\parallel e}}{\omega_{ce}}$ called as wave vector is introduced.

A more accurate representation of the true frequency and growth rate may be obtained when propagating electron cyclotron waves obliquely into the magnetic field:

$$\frac{\gamma}{\omega_{ce}}=\frac{\frac{\sqrt{\pi}}{\tilde{k}\cos\theta}\left(\frac{X_{2e}}{X_{1e}}-K_4\right)K_3^3\exp\left(-\left(\frac{K_3}{\tilde{k}\cos\theta}\right)^2\right)}{1+\frac{\tilde{k}^2\cos^2\theta}{2K_3^2}-\frac{\tilde{k}^2\cos^2\theta}{K_3}\left(\frac{X_{2e}}{X_{1e}}-K_4\right)-\frac{m_i}{m_e}\frac{X_{1e}}{X_{1i}}K_3^2} \quad (8)$$

The real part of eq. (8) is

$$X_3 = -\frac{\omega_r}{\omega_c} = X_4 + \frac{\tilde{k}^2 \cos^2\theta}{2\beta_1}\left[\frac{-(1+X_4)}{X_{1e}} + \frac{X_{2e}}{X_{1e}}\frac{\beta_1}{1+X_4}\right]$$

where $K_3 = 1 - X_3 + X_4$, $K_4 = \frac{X_3 - X_4}{K_3}$ and

$$\beta_1 = \frac{4\pi\mu_o\varepsilon_o k_b T_{\|i}(n_i/n)}{AB_o^2},\ X_4 = \frac{k_\| \Gamma_{\|i}}{\nu\omega_c} - \frac{p\nu}{\omega_c} \quad (9)$$

3. PLASMA PARAMETERS

During the Voyager flybys of Saturn's inner magnetosphere, plasma wave discharges up to 10 R_S in size and complexity were discovered. The magnetosphere of Saturn has revealed a plethora of plasma waves. According to Kurth & Gurnett (1991) and Zarka et al. (2004), Cassini discovered (Electron Cyclotron Harmonics) ECHs in the 1–8 R_S region. The Voyager 1 was detecting electron number densities and energetic hot-and-cold distributions distance between the radial distance 6 and 18 R_s. Over the same radial distance, the magnetic field strength varied from 80 to 4.4 nT (Sittler et al. 1983). Inner plasma torus parameters we calculated at radial distance 7 R_s to 5.5 R_s, B_0 = 100 nT, $n_o = 14 \times 10^6$ m^{-3}, $K_bT_\|$ = 20 eV (Akalin et al. 2006; Thomsen et al. 2010).In addition, the equation used to calculate the magnetic field intensity along magnetic field lines at any position:

$$B = B_0 \frac{\sqrt{1+3\sin^2\lambda}}{\cos^6\lambda}$$

Where λ is latitude and B_0 is the magnetic field at the equator, evaluated by using the measured magnetic field at spacecraft.

4. RESULT AND DISCUSSION

The dimensionless grow rate of EMEC waves changes with wave number ($\tilde{k}$) for various A.C frequency values, as shown in Figs. 1(a) and 1(b).

Plots were drawn at a radial distance of 5.5 R_s for two separate scenarios: without a model of magnetic field and with a magnetic field model. Fig. 1(a) has been plotted for without any model. For this case, maxima of growth rate lies at $\tilde{k}$ = 0.46 with $\gamma / \omega_c = 8.1 \times 10^{-3}$ for ν = 2 kHz and maxima shifts to $\tilde{k}$ = 0.5 for ν = 4 kHz with $\gamma / \omega_c = 8.6 \times 10^{-3}$. Peak value of growth rate lies at $\tilde{k}$ = 0.52 with $\gamma / \omega_c = 9.1 \times 10^{-3}$ for ν = 6 kHz. For Fig. 1(b), magnetic field model has been incorporated which is as discussed in previous section. Graph show that maximum growth rate occurs at $\tilde{k}$ = 0.44 with $\gamma / \omega_c = 8.2 \times 10^{-3}$ for ν = 2 kHz, and at and maxima shifts to $\tilde{k}$ = 0.5 for ν = 4 kHz with $\gamma / \omega_c = 8.8 \times 10^{-3}$. Peak value of growth rate lies at $\tilde{k}$ = 0.55 with $\gamma / \omega_c = 9.3 \times 10^{-3}$ for ν = 6 kHz. As the value of A.C. frequency grows, the growth rate increases. With the magnetic field model included for research, but for lower A.C. frequencies, we can see that the spectrum moves to a lower wave number [compare Figs. 1(a) and 1(b)]. As shown in the graphs above, the alternating current frequency activates electromagnetic electron cyclotron waves in the inner plasma torus, which expand at a faster pace as the frequency rises. An electromagnetic electron cyclotron wave growth rate normalized in a parallel

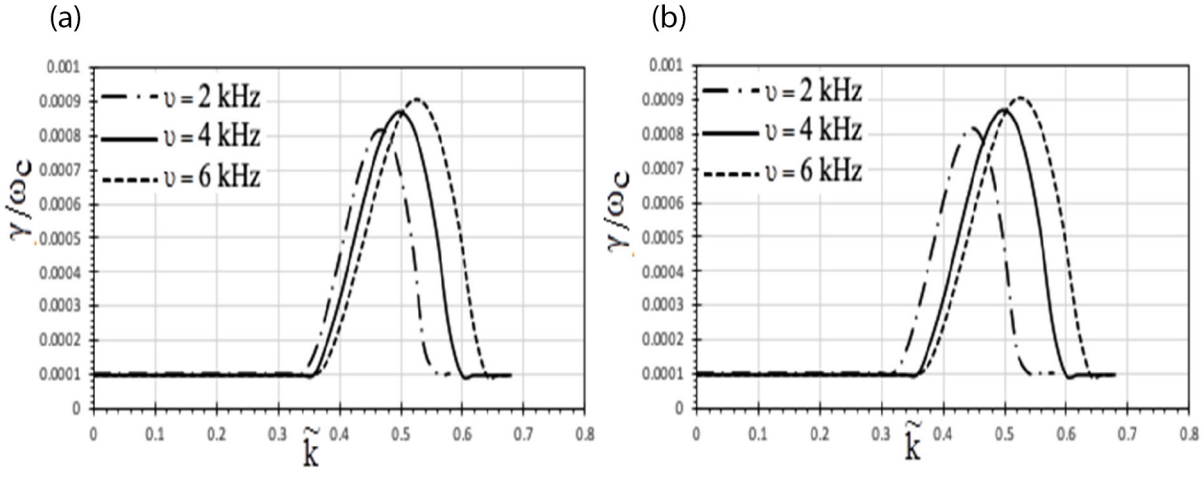

Fig. 1. Growth rate for without and with model for AC frequency. (a) Without model - keeping keeping $T_\perp / T_\| = 1.5$, $\theta = 10^o$, E_o = 0.1 mV/m, $n_o = 14 \times 10^6$ m^{-3}, and other plasma parameters constant. (b) With model - keeping $T_\perp / T_\| = 1.5$, $\theta = 10^o$, E_o = 0.1 mV/m, $n_o = 14 \times 10^6$ m^{-3}, and other plasma parameters constant. AC, alternating current.

AC field was employed by Pandey & Kaur (2015) to construct their graphs.

Figs. 2(a) and 2(b) shows the variation of dimensionless growth rate of EMEC waves with wave number ($\tilde{k}$) for different value of $T_\perp / T_\parallel$. From perpendicular to parallel, the thermal energy ratios are changed $T_\perp / T_\parallel - 1 = A_T$. The effect of temperature anisotropy (A_T) on the parallel energy ratio was investigated. Graphs have been displayed for the magnetic field model and non-magnetic field propagation in the oblique direction of the magnetic field at a radial distance of 5.5 R_S. In Fig. 2(a), the maxima of growth rate fall about $\tilde{k} = 0.5$ with for $T_\perp / T_\parallel = 1.25$, 1.5, and 1.75 at $\gamma / \omega_c = 8 \times 10^{-3}$, 8.75×10^{-3}, and 9.3×10^{-3} respectively. The growth maxima are different at this point for all the $T_\perp / T_\parallel$ values and maxim shifts to $\tilde{k} = 0.52$ for $T_\perp / T_\parallel = 1.25$ and $\tilde{k} = 0.48$ for $T_\perp / T_\parallel = 1.75$ Fig. 2(b), similar growth patterns are observed, but the maxima for $T_\perp / T_\parallel$ comes before $\tilde{k} = 0.5$. For Fig. 2(b), In this figure, the magnetic field dependence on latitude has been employed in calculations. The maximum is shown by the growth rate at $\tilde{k} = 0.5$ with $\gamma / \omega_c = 7.9 \times 10^{-3}$ for $T_\perp / T_\parallel = 1.25$, $\tilde{k} = 0.5$ with $\gamma / \omega_c = 8.6 \times 10^{-3}$ for $T_\perp / T_\parallel = 1.5$ and at $\tilde{k} = 0.48$ with $\gamma / \omega_c = 9.4 \times 10^{-3}$ for $T_\perp / T_\parallel = 1.75$.

Since the value of growth rate rises with increasing temperature anisotropy $T_\perp / T_\parallel$ (in both cases and at 5.5 radial distance), the growth rate rises as well. According to this comparison, the bandwidth of the growth rate has shrunk and the spectrum has shifted to a higher wave number for the value $T_\perp / T_\parallel = 1.25$, which has been used in research. For EMEC waves in the Earth's plasma pause zone, similar outcomes were found by Ahirwar (2012).

Figs. 3(a) and 3(b) show how the dimensionless growth rate of EMEC waves varies with wave number ($\tilde{k}$) for various propagation angles with respect to the planet's magnetic field. The maximum for the scenario where no model has been examined are in the range of $\gamma / \omega_c = 8.6 \times 10^{-3}$ to 8.7×10^{-3} for $\tilde{k} = 0.5$ to 0.56. The maximum growth rate is nearly the same when the effect of the magnetic field model is incorporated when the angle of propagation advances to 30°. In Fig. 3(b), the growth rate peak coincides at same $\tilde{k} = 0.5$ for angle of propagation of 10° and 20°. As the graphs show, changing the propagation angle has little to no impact on wave growth. Due to the magnetic field model's effect, the wave can only develop at one particular wavenumber. When the wave normal angle is increased from 10° to 30°, the growth rate also increases. Above 40°, electrostatic components take the place of electromagnetic components, and non-resonant instability kicks in.

Figs. 4(a) and 4(b) show how the dimensionless development rate of EMEC waves which varies with wave number ($\tilde{k}$) for different electric field magnitudes. (E_0).

Fig. 4(a) demonstrates how the EMEC wave's maximum growth rate fluctuates with the electric field's intensity vs. the number of waves. Wave growth increases as the electric field strength increases, as shown in the diagram. For $E_0 = 0.3$ mV/m, maxima $\gamma / \omega_c = 9.1 \times 10^{-3}$ occurs at $\tilde{k} = 0.58$, showing maximum growth. For $E_0 = 0.2$ mV/m, $\gamma / \omega_c = 8.9 \times 10^{-3}$ maxima appears at $\tilde{k} = 0.57$ and for $E_0 = 0.1$ mV/m, the growth rate peaks at 8.6×10^{-3} in oblique propagation case shifted to $\tilde{k} = 0.5$. Modeling the impact of the magnetosphere's EMEC wave growth using a magnetic field model is shown in Fig. 4(b). On comparing two, it is observed that the growth rates are similar, but the apex sites differ slightly. Because maximal growth rates are influenced

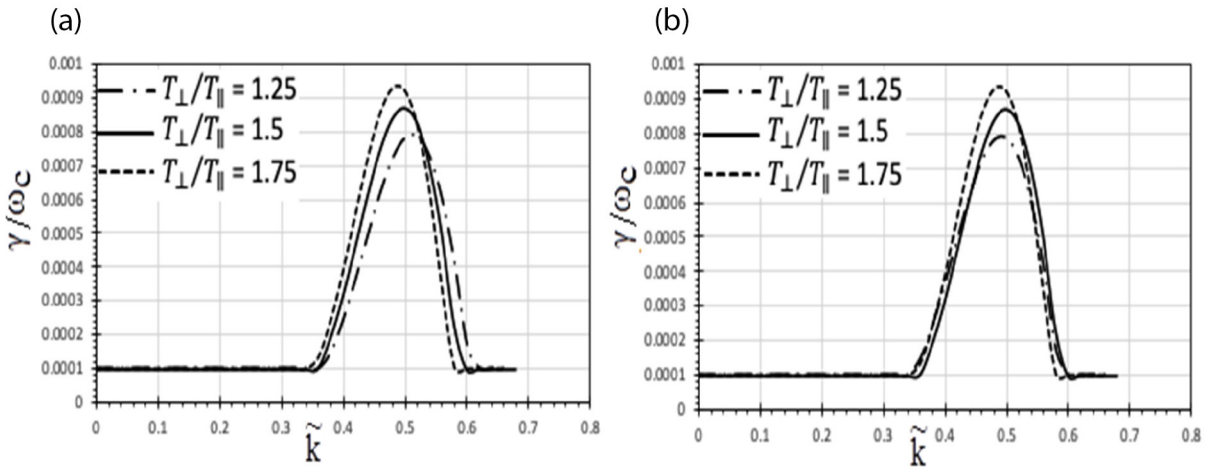

Fig. 2. Growth rate for without and with model for perpendicular and parallel temperature ratio. (a) Without model - keeping $\upsilon = 4$ kHz, $\theta = 10^\circ$, $E_o = 0.1$ mV/m, $n_o = 14 \times 10^6$ m^{-3}, and other plasma parameters constant. (b) With model - keeping $\upsilon = 4$ kHz, $\theta = 10^\circ$, $E_o = 0.1$ mV/m, $n_o = 14 \times 10^6$ m^{-3}, and other plasma parameters constant.

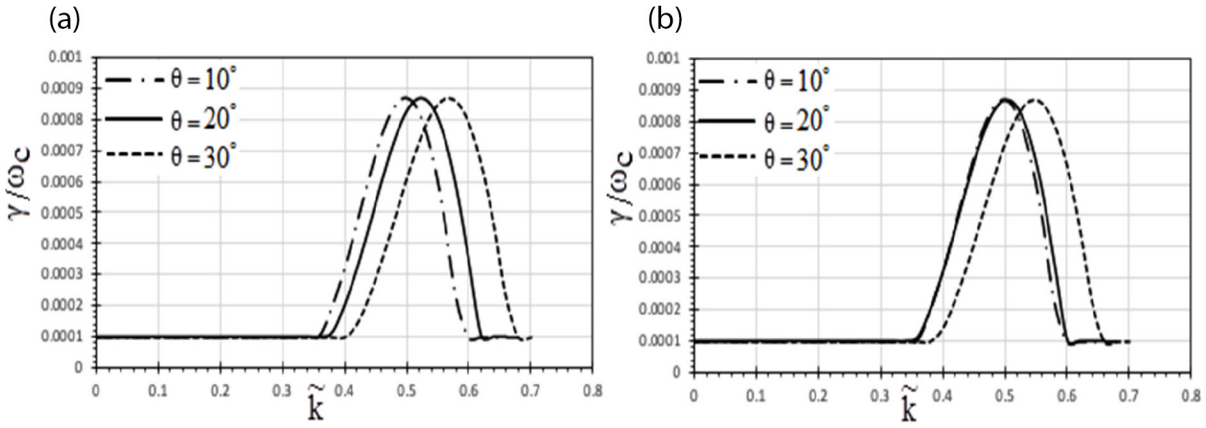

Fig. 3. Growth rate for without and with model for Propagation angle. (a) Without model - keeping $T_{\perp} / T_{\parallel} = 1.5$, $E_o = 0.1$ mV/m, $n_o = 14 \times 10^6$ m^{-3}, $\upsilon = 4$ kHz and other plasma parameters constant. (b) With model - keeping $T_{\perp} / T_{\parallel} = 1.5$, $E_o = 0.1$ mV/m, $n_o = 14 \times 10^6$ m^{-3}, $\upsilon = 4$ kHz and other plasma parameters constant.

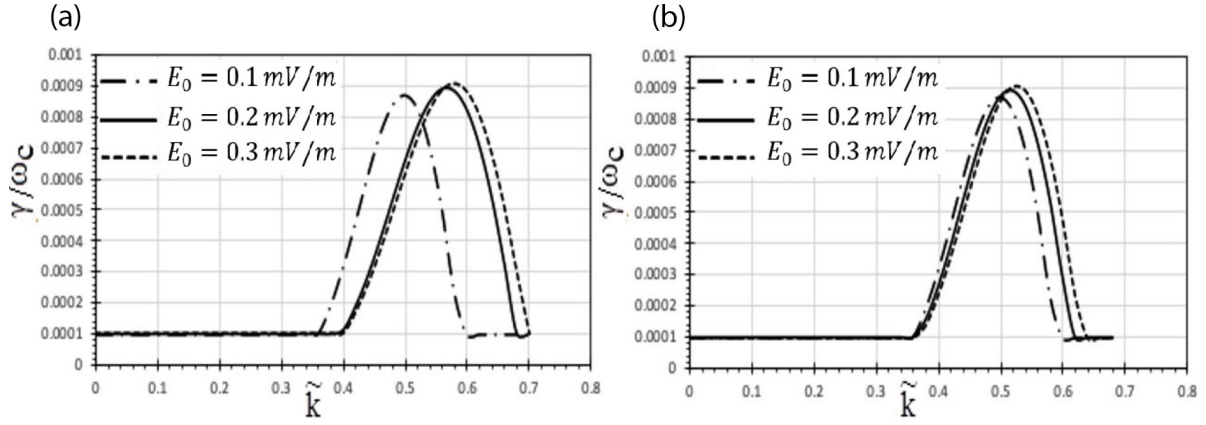

Fig. 4. Growth rate for without and with model for magnitude of AC electric field. (a) Without model - keeping $T_{\perp} / T_{\parallel} = 1.5$, $n_o = 14 \times 10^6$ m^{-3}, $\theta = 10^{\circ}$, $\upsilon = 4$ kHz and other plasma parameters constant. (b) With model - keeping $T_{\perp} / T_{\parallel} = 1.5$, $n_o = 14 \times 10^6$ m^{-3}, $\theta = 10^{\circ}$, $\upsilon = 4$ kHz and other plasma parameters constant. AC, alternating current.

by electric field intensity, particles may oscillate at different frequencies and absorb energy to grow waves. Kumari & Pandey (2019).

5. CONCLUSION

According to this article, Saturn's inner plasma torus has high growth rates of electron cyclotron waves. A mathematical model based on the ring distribution function could yield growth rate expressions derived to the dispersion relation. Instability in the magnetosphere can be studied using this technique. These charts demonstrate that in Saturn's magnetosphere, temperature anisotropy serves as a free energy source. Increases in the electric field's amplitude and alternating current (AC) frequency hasten the creation of electron cyclotron waves. The loss of perpendicular kinetic energy has increased the magnitude of electromagnetic electron cyclotron waves. There is no doubt that raising the magnetic field model's dimensionless growth rate has an impact on parameters with lower values of the magnetic field. In case of the magnetic model, the growth rate increases marginally as compare to without the magnetic model, but the band width has been increased in case of a magnetic field model, it means the spectrum covers a wide frequency range. Saturnian magnetosphere VLF (very low frequency) emissions may now be studied across a wider frequency range because of the shift in wave number. This research could be used to understand more about Saturn's outer radiation belt, whistler mode wave expansion, and other spatial plasmas. EMEC wave studies at higher latitudes, which are thought to be linked

to critical high-temperature anisotropies, can be extended to examine pitch angle scattering mechanisms changing plasma characteristics and local loss processes in the inner magnetosphere, which are other ideas we propose for future work in this area.

ACKNOWLEDGMENTS

The authors are grateful to Dr. Ashok K. Chauhan (Founder President, Amity University), Dr. Atul Chauhan (President, Amity University) and Dr. Balvinder Shukla (Vice Chancellor, Amity University) for their immense encouragement. We also express our gratitude to the reviewers for their expert comments for the manuscript.

ORCIDs

Annex Edappattu Haridas https://orcid.org/0000-0002-5193-6795
Shifali Kanwar https://orcid.org/0000-0002-8869-2165
Rama Shankar Pandey https://orcid.org/0000-0003-4907-1080

REFERENCES

Ahirswar G, Study of electromagnetic electron cyclotron waves around plasma-pause region, Res. J. Eng. Sci. 1, 18 (2012).

Akalin F, Gurnett DA, Averkamp TF, Persoon AM, Santolik O, et al., First whistler observed in the magnetosphere of Saturn, Geophys. Res. Lett. 33, L20107 (2006). https://doi.org/10.1029/2006GL027019

André N, Dougherty MK, Russell CT, Leisner JS, Khurana KK, Dynamics of the Saturnian inner magnetosphere: first inferences from the Cassini magnetometers about small-scale plasma transport in the magnetosphere, Geophys. Res. Lett. 32, L14S06 (2005). https://doi.org/10.1029/2005GL022643

Annex EH, Pandey RS, Generation of oblique electromagnetic wave by hot injection electron beam with parallel AC electric field in the magnetosphere of Saturn, Astrophys. Space Sci. 364, 81 (2019). https://doi.org/10.1007/s10509-019-3566-4

Chou M, Cheng CZ, Distribution of water-group ion cyclotron waves in Saturn's magnetosphere, Earth Planets Space. 69, 122 (2017). https://doi.org/10.1186/s40623-017-0709-0

Delamere PA, Bagenal F, Modeling variability of plasma conditions in the Io torus, J. Geophys. Res. Space Phys. 108, 127 (2003). https://doi.org/10.1029/2002JA009706

Eviatar A, Siscoe GL, Scudder JD, Sittler EC Jr, Sullivan JD, The plumes of Titan, J. Geophys. Res. Space Phys. 87, 8091-8103 (1982). https://doi.org/10.1029/JA087iA10p08091

Goertz CK. Detached plasma in Saturn's front side magnetosphere, Geophys. Res. Lett. 10, 455-458 (1983). https://doi.org/10.1029/GL010i006p00455

Gurnett DA, Bhattacharjee A, Introduction to Plasma Physics (Cambridge University Press, Cambridge, UK, 2005).

Gurnett DA, Kurth WS, Scarf FL, Plasma waves near Saturn: initial results from Voyager 1, Science 212, 235-239 (1981). https://doi.org/10.1017/CBO9780511809125

Horner J, Kane SR, Marshall JP, Dalba PA, Holt TR, et al., Solar system physics for exoplanet research, Publ. Astron. Soc. Pac. 132, 102001 (2020). https://iopscience.iop.org/article/10.1088/1538-3873/ab8eb9

Kumar S, Singh SK, Gwal AK, Effect of upflowing field-aligned electron beams on the electron cyclotron waves in the auroral magnetosphere, Pramana J. Phys. 68, 611-622 (2007). https://doi.org/10.1007/s12043-007-0063-z

Kumari J, Pandey RS, Study of VLF wave with relativistic effect in Saturn magnetosphere in the presence of parallel A.C. electric field, Adv. Space Res. 63, 2279-2289 (2019). https://doi.org/10.1016/j.asr.2018.12.013

Kurth WS, Gurnett DA, New observations of the low frequency interplanetary radio emissions, Geophys. Res. Lett. 18, 1801-1804 (1991). https://doi.org/10.1029/91GL02309

Lacombe C, Alexandrova O, Matteini L, Santolík O, Cornilleau-Wehrlin N, et al., Whistler mode waves and the electron heat flux in the solar wind: cluster observations, Astrophys. J. 796, 5 (2014). https://doi.org/10.1088/0004-637X/796/1/5

Pandey RS, Kaur R, Oblique electromagnetic electron cyclotron waves for kappa distribution with AC field in planetary magnetospheres, Adv. Space Res. 56, 714-724 (2015). https://doi.org/10.1016/j.asr.2015.04.032

Pandey RS, Pandey RP, Srivastava AK, Karim SM, Hariom, The electromagnetic ion-cyclotron instability in the presence of A.C. electric field for lorentzian kappa, Prog. Electromagn. Res. M. Pier M. 1, 207-217 (2008). https://doi.org/10.2528/PIERM08032601

Richardson JD, Sittler EC Jr, A plasma density model for Saturn based on Voyager observations, J. Geophys. Res. Space Phys. 95, 12019-12031 (1990). https://doi.org/10.1029/JA095iA08p12019

Sittler EC Jr, Ogilvie KW, Scudder JD, Survey of low-energy plasma electrons in Saturn's magnetosphere: Voyagers 1 and 2, J. Geophys. Res. Space Phys. 88, 8847-8870 (1983). https://doi.org/10.1029/JA088iA11p08847

Thomsen MF, Reisenfeld DB, Delapp DM, Tokar RL, Young DT, et al., Survey of ion plasma parameters in Saturn's magnetosphere, J. Geophys. Res. Space Phys. 115, A10220

(2010). https://doi.org/10.1029/2010JA015267
Wu CS, Yoon PH, Freund HP, A theory of electron cyclotron waves generated along auroral field lines observed by ground facilities, Geophys. Res. Lett. 16, 1461-1464 (1989). https://doi.org/10.1029/GL016i012p01461
Zarka P, Cecconi B, Kurth WS, Jupiter's low-frequency radio spectrum from Cassini/radio and plasma wave science (RPWS) absolute flux density measurements, J. Geophys. Res. Space Phys. 109, A09S15 (2004). https://doi.org/10.1029/2003JA010260